

Geodetic slip rate for the eastern California shear zone and the recurrence time of Mojave desert earthquakes

Jeanne Sauber*, Wayne Thatcher†, Sean C. Solomon‡ & Michael Lisowski†

* Geodynamics Branch, Laboratory for Terrestrial Physics, NASA Goddard Space Flight Center, Greenbelt, Maryland 20771, USA

† US Geological Survey, Menlo Park, California 94025, USA

‡ Department of Terrestrial Magnetism, Carnegie Institution of Washington, Washington DC 20015, USA

WHERE the San Andreas fault passes along the southwestern margin of the Mojave desert, it exhibits a large change in trend, and the deformation associated with the Pacific/North American plate boundary is distributed broadly over a complex shear zone. The importance of understanding the partitioning of strain across this region, especially to the east of the Mojave segment of the San Andreas in a region known as the eastern California shear zone (ECSZ), was highlighted by the occurrence (on 28 June 1992) of the magnitude 7.3 Landers earthquake in this zone. Here we use geodetic observations in the central Mojave desert to obtain new estimates for the rate and distribution of strain across a segment of the ECSZ, and to determine a coseismic strain drop of ~ 770 μrad for the Landers earthquake. From these results we infer a strain energy recharge time of 3,500–5,000 yr for a Landers-type earthquake and a slip rate of ~ 12 mm yr^{-1} across the faults of the central Mojave. The latter estimate implies that a greater fraction of plate motion than heretofore inferred from geodetic data is accommodated across the ECSZ.

Although most of the relative motion between the Pacific and North American tectonic plates in the southwestern United States occurs by slip on the San Andreas fault, there are numerous other faults that have slipped in the past million years^{1,2}. Very-long-baseline-interferometry (VLBI) measurements made since 1984 (Fig. 1) and conventional laser ranging measurements begun in 1971 (ref. 3) show that 75% of the continuing motion between the Pacific and North American plates is distributed across a zone ~ 100 km wide in southernmost California. The strike of the San Andreas fault is approximately parallel to the slip direction of relative plate motion, N33–41° W (ref. 4), along most parts of the plate boundary. But along a 190-km-long segment between San Gorgonio Pass and Tejon Pass (referred to here as the Mojave segment) the San Andreas fault locally changes its trend by 20° to 30° (Fig. 1). Across this segment of the plate boundary, the width of the zone accommodating a comparable fraction of plate motion is broader (~ 200 km) and the mode of deformation is more complex (Fig. 1). To the northeast of the Mojave segment of the San Andreas fault are the right-lateral strike-slip faults of the Mojave desert (Fig. 1). Palaeoseismic⁵, geological⁶, and geodetic^{7,8,9} observations suggest the presence of a zone of shear-strain accumulation which extends from the San Gorgonio Pass to north of the Garlock fault in eastern California, known as the eastern California shear zone (ECSZ). Aftershocks from the Landers earthquake and an adjacent magnitude 6.1 event in April 1992 defined a seismic lineament >80 km long within the ECSZ.

The central Mojave geodetic network spans a segment of the ECSZ from west of the Helendale fault to east of the Ludlow fault and includes the northern segment of the Landers earthquake rupture (Fig. 1). We have determined the rate and spatial distribution of continuing strain for a number of different spatial subnets using a moving-window approach. An earlier analysis of the same data⁷ was adversely affected by a poor

eccentric reduction between observations made in 1935 and those made in 1965 and 1982 at a station just east of the Camp Rock fault, and by three angles with unusually large angle changes (>4 arcsec) involving a station just east of the Pisgah fault. Whereas the earlier analysis⁷ suggested that an abrupt decrease in the rate of shear strain occurs to the east of the Camp Rock fault (Fig. 1), our new results (with the poor data removed) suggest that active strain accumulation extends at least between the Helendale and Pisgah faults, a zone ~ 60 km wide. Between the Pisgah and Ludlow faults we were unable to discern a significant strain rate (Table 1). The average shear-strain rate between the Helendale and Pisgah faults during 1934–82 was $\dot{\gamma} = 0.15 \pm 0.03$ $\mu\text{rad yr}^{-1}$, with the maximum right-lateral shear strain occurring on a plane oriented N39° W $\pm 5^\circ$. Geological observations suggest that a small component of north-south contraction accompanies slip on the northwest-striking faults¹⁰. The geodetic observations from the central Mojave network

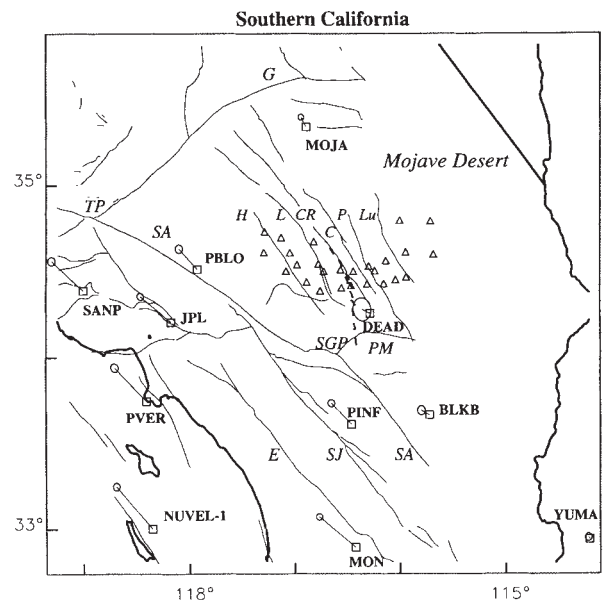


FIG. 1 The location of the stations in the central Mojave geodetic network (triangles), the 28 June 1992 Landers earthquake rupture (dashed line)²⁶, and the vector velocity of western US sites (squares) and associated 95% confidence ellipses estimated from VLBI measurements. We determined site velocities from VLBI data²⁷ taken over the period 1984–91 in a reference frame defined by minimizing the velocity of reference sites (North American plate: Haystack and Westford, Massachusetts; Pietown, New Mexico; Platteville, Colorado; Gilcreek, Alaska. Pacific plate: Kauai, Hawaii; Vandenberg, California. Eurasian plate: Wettzell, Germany; Onsala, Sweden.) with respect to the predicted NUVEL-1 (ref. 4) velocity in a frame in which North America is fixed. The slip direction and rate (49.6 ± 1.3 mm yr^{-1}) of Pacific plate motion with respect to the North American plate predicted by the global plate motion model NUVEL-1 is given in the lower left corner. Faults or fault zones¹: C, Calico; CR, Camp Rock-Emerson; E, Elsinore; G, Garlock; H, Helendale; L, Lenwood; Lu, Ludlow; PM, Pinto Mountain; P, Pisgah; SA, San Andreas; SJ, San Jacinito. Other features: SGP, San Gorgonio Pass; TP, Tejon Pass. The velocities of some of the VLBI stations, with their 1σ uncertainties are: DEAD, 7.7 ± 3.4 mm yr^{-1} at N62° W $\pm 15^\circ$; MOJA, 9.5 ± 1.1 mm yr^{-1} at N26° W $\pm 3^\circ$; PBLO, 24.4 ± 1.4 mm yr^{-1} at N41° W $\pm 2^\circ$; YUMA, 1.8 ± 1.3 mm yr^{-1} at N34° W $\pm 20^\circ$. The differenced velocity vector between MON and BLKB is 33.5 ± 1.9 mm yr^{-1} at N48° W $\pm 2^\circ$, between MON and YUMA is 39.4 ± 1.7 mm yr^{-1} at N50° W $\pm 1^\circ$, between JPL and PBLO is 11.1 ± 1.8 mm yr^{-1} at N67° W $\pm 5^\circ$, between JPL and MOJA is 26.2 ± 1.6 mm yr^{-1} at N57° W $\pm 2^\circ$, and between PVER and MOJA is 31.3 ± 1.8 mm yr^{-1} at N48° W $\pm 2^\circ$.

TABLE 1 Rate and orientation of maximum right-lateral shear strain, central Mojave network, 1934–82

Region	No. of obs.	$\dot{\gamma}$ ($\mu\text{rad yr}^{-1}$)	ψ (degrees)
Helendale/Lenwood	28	0.14 ± 0.04	-45 ± 12
Camp Rock	12	0.16 ± 0.06	-44 ± 9
Landers rupture	10	0.22 ± 0.09	-42 ± 7
Calico/Pisgah	12	0.15 ± 0.06	-28 ± 15
Pisgah/Ludlow	18	0.06 ± 0.06	unresolved
Helendale/Pisgah	69	0.15 ± 0.03	-39 ± 5
Helendale/Ludlow	92	0.14 ± 0.03	-43 ± 5

The maximum horizontal shear-strain rate is denoted by $\dot{\gamma}$, and ψ (positive clockwise from N) is the azimuth of maximum right-lateral shear strain for subnetworks straddling the named faults. Angle changes over the period 1934–82 were obtained from historical triangulation measurements made between 1934 and 1940 and again in 1965 and trilateration measurements made in 1982. To estimate strain rates, angle changes between successive surveys were fitted to a strain-rate field assumed to be spatially and temporally uniform using a modified version of Frank's method²⁵.

indicate that the axis of maximum compressional strain is orientated N06° W \pm 5°, similar to the observed direction of contraction across local folds (A. Glazner, personal communication). As geological data and recent trenching studies^{11,12} indicate large right-lateral displacements along faults trending north-to-northwest, and right-lateral slip occurred on some of these faults in the Landers event, $\dot{\gamma}$ is most simply interpreted as representing right-lateral shear strain.

The geodetically measured strain rate in the central Mojave desert could be due to one or more of several different mechanisms: (1) earthquakes, (2) fault creep, (3) elastic strain, or (4) anelastic processes such as folding. We had postulated earlier that most of the measured strain between the Helendale and Camp Rock faults was the result of either elastic strain accumulation or fault creep⁷. Although a part of the observed straining across the western part of the central Mojave network could be due to strain accumulation across the San Andreas fault, the magnitude of this effect is uncertain. A dislocation model of the San Andreas fault with a locking depth of 20 km (the maximum depth of seismicity¹³) and a slip rate of 30 mm yr⁻¹ (ref. 14) suggests that elastic strain associated with the San Andreas fault could account for as much as 30% of strain rate in the Helendale/Lenwood subnetwork but <10% of that across the Calico/Pisgah subnetwork. The amount of this San Andreas contribution depends on uncertain modelling assumptions, and so we have made no attempt to correct for it in what follows. If significant, its effect would be to decrease estimates of cumulative slip across central Mojave faults and increase estimates of strain recharge times across the Landers rupture. That the rupture during the Landers earthquake extended across numerous fault segments confirms that the strain rate measured over a broad region in the Mojave desert is released, at least in part, by large Mojave earthquakes. An independent assessment of the seismic hazard in southern California based on geological offsets also led to the suggestion that major earthquakes (with magnitude up to ~6.9) would occur on individual fault segments of the Mojave desert¹⁵.

Within the brittle upper crust, tectonic motion across a plate boundary is accommodated primarily by earthquakes or episodic creep. Below the seismogenic zone, slip has been hypothesized to occur aseismically on a downward extension of individual faults, or as a broad shear zone below the surface trace of several faults¹⁶. A shear zone model with multiple discrete faults underlain by a zone of distributed ductile deformation can be used to represent the rate and distribution of strain in the central Mojave and to estimate an equivalent slip rate across the shear zone. The engineering shear-strain rate $\dot{\gamma}$ at the surface is related to the distance x from the centre of the

shear zone by¹⁶:

$$\dot{\gamma} = \frac{-\dot{b}}{2\pi W} \left(\tan^{-1} \frac{x-W}{D} - \tan^{-1} \frac{x+W}{D} \right)$$

where \dot{b} is the slip rate across the zone of deformation, D is the depth of the shear zone, and W is the half-width of the shear zone. The depth of background seismicity (the maximum focal depth is 15 km, and most events are at <6 km (ref. 7) and Landers aftershocks¹⁷ and the depth extent of the Landers rupture on the northern segment (less than 10 km^{18,19,20}) constrain the depth of the transition from brittle to ductile behaviour to be ~10–15 km. Two distributed shear-strain models that are consistent with the 1 standard deviation (1 σ) uncertainties in the central Mojave data are depicted in Fig. 2. The slip rate in the models that fit the data (with $D=10$ –15 km, $W=30$ km) varies from 10 to 14 mm yr⁻¹. A slip rate estimate of about 12 mm yr⁻¹ across a 60-km-wide zone is consistent with geological data that suggest a slip rate over the past 5.5 Myr of 12 mm yr⁻¹ (ref. 6). Earlier geodetic estimates of the slip rate were lower, 7–8 mm yr⁻¹, and were obtained by simply multiplying the average strain rate by the width of the zone of strain accumulation, taken to be between 40 and 60 km (refs 7, 8).

In principle, the amount of time required to accumulate strain energy equivalent to that released in a given earthquake can be calculated by comparing the coseismic strain release with the rate of interseismic strain accumulation^{21,22}. We used angle changes measured between 1934 and 1982 at four sites that spanned the Landers rupture (Fig. 1) to estimate a rate of interseismic strain of $\dot{\gamma} = 0.22 \pm 0.09 \mu\text{rad yr}^{-1}$ (Table 1), a result not significantly higher than in adjacent segments of the shear zone. The average

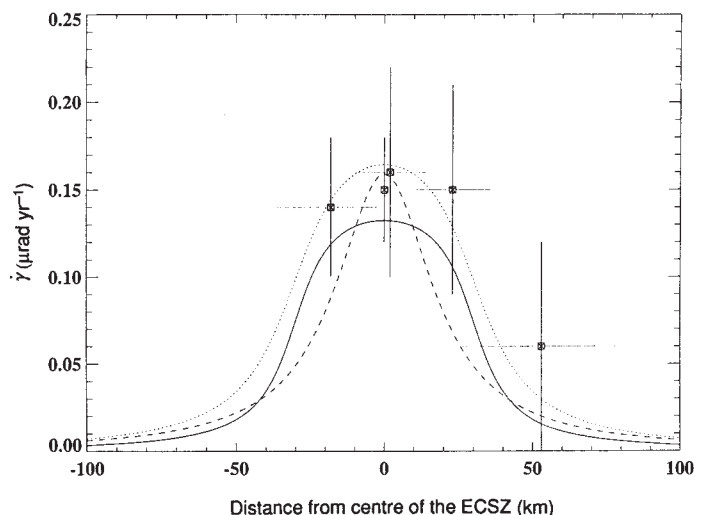


FIG. 2 Predicted and calculated shear-strain rate ($\dot{\gamma}$) plotted against distance from the centre of the eastern California shear zone (taken here to be half way between the Helendale and Pisgah faults); distances to the east and west are shown as positive and negative respectively. The shear-strain rate for the subnetworks and the average strain rate between the Helendale and Pisgah faults (Table 1) are given by squares; vertical error bars represent 1 σ . The approximate width of the four subregions is indicated by horizontal error bars. The predicted shear-strain rate for the distributed shear-strain model with a total width of 60 km ($W=30$) is given by the solid line for $D=10$ km and $\dot{b}=10$ mm yr⁻¹ and by the dotted line for $D=15$ km and $\dot{b}=14$ mm yr⁻¹. For comparison, the shear-strain rate predicted for 10 mm yr⁻¹ of slip on a single fault at a depth of 20 km (ref. 8) is given by the dashed line. The average strain rate across the Barstow trilateration network⁸, northeast of the central Mojave network, and spanning ~50 km is $0.13 \pm 0.02 \mu\text{strain yr}^{-1}$ at N33° W \pm 4°.

shear-strain change across the Landers rupture between 1982 (when trilateration measurements were made) and July 1992 Global Positioning System measurements was $\sim 767 \mu\text{rad}$, more than a factor of 10 larger than the average coseismic strain drop for earthquakes of $\sim 50 \mu\text{rad}$ suggested by Rikitake²². Taking the ratio of the Landers coseismic strain drop ($767 \mu\text{rad}$) to the interseismic strain rate across the same region ($0.22 \mu\text{rad yr}^{-1}$) gives a strain recharge time of $\sim 3,500$ yr, or $\sim 5,000$ yr if we use the Camp Rock subnetwork (Table 1). The difficulty in using the strain energy recharge method to estimate a recurrence interval is that the size of the expected earthquake and the amount of interseismic strain associated with a single Mojave fault are uncertain. Independent palaeoseismic^{5,11,12} and seismic hazard studies¹⁵ suggest a recurrence time for individual earthquakes on Mojave faults of thousands to tens of thousands of years. In contrast, the time interval between the last 10 earthquakes on the Mojave segment of the San Andreas fault is between ~ 40 and 330 yr (ref. 23). Although the repeat time for individual earthquakes in the Mojave desert may be 10^3 or 10^4 yr, there are multiple faults that accommodate a slip rate that we estimate to be $\sim 1/3$ that of the adjacent San Andreas fault. Therefore, an earthquake would be expected somewhere within the central Mojave more frequently than the strain energy recharge rate for an individual event.

A long-term slip rate across the Mojave shear zone of $\sim 12 \text{ mm yr}^{-1}$ implies that the remaining relative plate motion of $\sim 34 \text{ mm yr}^{-1}$ (ref. 4) is accommodated by slip on, or to the west of, the San Andreas fault. Ground-based geodetic and VLBI data are consistent with this inference. From a dislocation model of the San Andreas fault in which the fault is locked below a depth of 20 km, ground-based geodetic data from the Mojave segment

imply a slip rate of $25 \pm 5 \text{ mm yr}^{-1}$ (ref. 24). A slip rate of $\sim 25 \text{ mm yr}^{-1}$ on this segment of the San Andreas fault, at the lower end of the generally cited range¹², is also consistent with similar modelling of the difference velocity observed between VLBI sites PBLO and JPL (Fig. 1). □

Received 27 April; accepted 12 November 1993.

- Jennings, C. W. Open-file Report No. 92-03 (Calif. Div. of Mines and Geol., Sacramento, 1992).
- Clark, M. M. et al. Open-file Report No. OFR-84-106 (US Geol. Surv., Reston, 1984).
- Lisowski, M., Savage, J. C. & Prescott, W. H. *J. geophys. Res.* **96**, 8369–8389 (1991).
- DeMets, C., Gordon, R. G., Argus, D. F. & Stein, S. *Geophys. J. Int.* **101**, 425–478 (1990).
- Wallace, R. E. *J. geophys. Res.* **89**, 5763–5769 (1984).
- Dokka, R. K. & Travis, C. J. *Geophys. Res. Lett.* **17**, 1323–1326 (1990).
- Sauber, J., Thatcher, W. & Solomon, S. C. *J. geophys. Res.* **91**, 12683–12693 (1986).
- Savage, J. S., Lisowski, M. & Prescott, W. H. *Geophys. Res. Lett.* **17**, 2113–2116 (1990).
- Sauber, J. thesis, Massachusetts Inst. of Technol. (1988); also as Technical memor. No. 100732 (NASA, Washington DC, 1989).
- Bartley, J. M., Glazner, A. F. & Schermer, E. R. *Science* **248**, 1398–1401 (1990).
- Lindvall, S. C. & Rockwell, T. K. *Geol. Soc. Am. Abstr. Prog.* **25(5)**, 70 (1993).
- Cinti, F. R. et al. *Geol. Soc. Am. Abstr. Progr.* **25(5)**, 21 (1993).
- Jones, L. M. *J. geophys. Res.* **93**, 8869–8891 (1988).
- Open File Report No. 88-398 (US Geol. Surv., Reston, 1988).
- Wesnousky, S. G. *J. geophys. Res.* **91**, 12587–12631 (1986).
- Prescott, W. H. & Nur, A. *J. geophys. Res.* **86**, 999–1004 (1981).
- Zhao, D. & Kanamori, H. *Geophys. Res. Lett.* **20**, 1083–1086 (1993).
- Murray, M. H., Savage, J. C., Lisowski, M. & Gross, W. K. *Geophys. Res. Lett.* **20**, 623–626 (1993).
- Blewitt, G. et al. *Nature* **361**, 340–342 (1993).
- Bock, Y. et al. *Nature* **361**, 337–339 (1993).
- Scholz, C. H. *The Mechanics of Earthquakes and Faulting* (Cambridge Univ. Press, 1990).
- Rikitake, T. *Earthquake Prediction* (Elsevier, Amsterdam, 1976).
- Sieh, K. E., Stuiver, M. & Brillinger, D. *J. geophys. Res.* **94**, 603–623 (1989).
- Eberhart-Phillips, D., Lisowski, M. & Zoback, M. D. *J. geophys. Res.* **95**, 1139–1153 (1990).
- Prescott, W. H. *Bull. Seism. Soc. Am.* **66**, 1847–1853 (1976).
- Seih, K. E. et al. *Science* **260**, 171–176 (1993).
- Ryan, J. W., Ma, C. & Caprette, D. S. Technical Memor. No. 104572 (NASA, Washington DC, 1993).

Sex ratio bias, relatedness asymmetry and queen mating frequency in ants

Liselotte Sundström

Department of Zoology, University of Helsinki, PO Box 17, FIN-00014 Helsinki, Finland

HAMILTON'S rule and the principle of inclusive fitness¹ provide a theoretical basis for understanding the evolution of social behaviour, and a framework for predicting reproductive characteristics of social insect colonies^{2–4}. Sex allocation in social insects (especially ants) has become a central factor in tests of inclusive fitness theory^{5–9}. The most powerful such test is the analysis of individual colonies where the predicted sex allocation varies depending on variation in worker fitness functions^{10,11}. Recently developed models^{5,12} predict that workers may enhance their inclusive fitness by biasing sex ratios in response to the degree of relatedness asymmetry in each colony. Here I provide the first empirical evidence of facultative sex ratio biasing in response to relatedness asymmetries caused by inter-colony variations in queen mating frequencies. In a Finnish population of the ant *Formica truncorum*, colonies have a single queen mated to one or several males. Colonies show a bimodal distribution of sex ratios, with a significantly greater proportion of males in colonies headed by a multiply mated queen.

The general prediction of inclusive fitness theory, that partial or complete worker control of sex allocation leads to overall female-biased sex ratios², agrees generally with empirical data^{6,7,13}. However, complications in the interpretation remain because a population level approach leaves the abundant variation in sex ratios among colonies unexplained¹⁴. Recent sex allo-

cation theory deals specifically with such inter-colony variation in sex ratios. Three mutually non-exclusive mechanisms have been proposed to explain colony level variation in sex ratios of social Hymenoptera. First, variations in resource levels may shift colony sex ratios towards male or female bias^{11,15}; second, differential dispersal of the sexes may result in different degrees of local mate competition or local resource competition^{16–18}, causing small colonies to specialize in one sex and large colonies to specialize in the other; and third, colonies with a high relatedness asymmetry are predicted to specialize in females and those with a lower relatedness asymmetry to specialize in males^{5,12,19}. (In Hymenoptera the haplodiploid sex-determining mechanism causes females to be on average more closely related to their sisters than to their brothers, compared with males; this is expressed as the relatedness asymmetry within a colony^{1,2,12}.) The first two hypotheses address factors associated with colony size and productivity, whereas the last model predicts an association between colony-specific relatedness structure and the sex ratio.

Observed sex-allocation patterns in halictid bees with eusocial and parasocial colonies^{20,21} and in some polygynous ants^{6,8} follow the predictions of relatedness-induced split sex ratio theory^{5,10,12}. In these cases, workers may assess the status of their colony by the presence or absence of a queen or by the presence of different numbers of functional queens. It has remained unclear, however, whether split sex ratio could work in cases where the variation in relatedness asymmetry is due solely to variation in queen mating frequencies. Here the assessment of colony type by investing workers would have to rely on some phenotypic expression of genetic diversity among nestmates, for example, genetically determined odour cues^{5,12,19,22}. Workers may control sex allocation both by selectively rearing or killing female and male larvae, and by nutritional control causing some female larvae to enter the queen development pathway while others develop into workers^{2,23,24}.